Chapter 3A

Interaction of Sinapic acid with calf thymus DNA

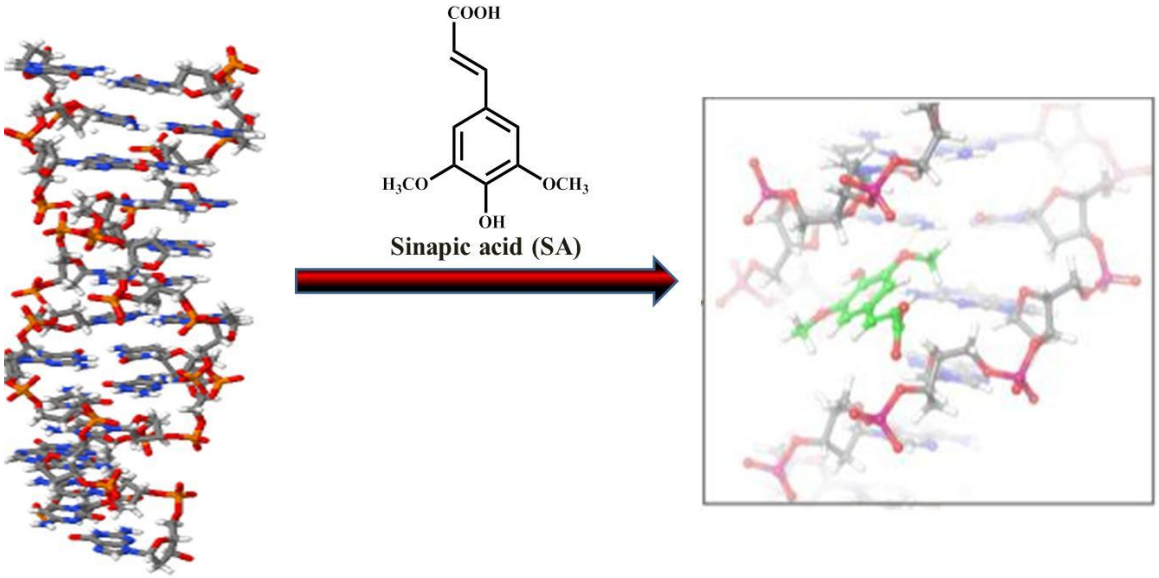

3A.1. Introduction

Currently, the study of the interaction of deoxyribonucleic acid (DNA) with small molecules is of immense interest in the arena of pharmaceutical chemistry [Mati et al., 2013]. DNA controls heredity of life in the living organism and is involved in essential biological process such as mutagenesis, gene transcription, gene expression, carcinogenesis and cell death, that makes them interesting to many researchers [Mati et al., 2013; Paul et al., 2011; Ma et al., 2012; Fei et al., 2009; Li et al., 2012; Jana et al., 2012]. According to literature the binding affinity and sequence specificity of small molecules with DNA depends on the various structural and electronic factors [Mati et al., 2013; Husain et al., 2017]. In this respect it is important to understand the binding affinities and binding mechanism between small molecules and DNA in modern clinical research.

Being a naturally occurring biologically significant molecule, phenolic acids are elaborately studied in the field of small molecule-DNA interaction. Phenolic acid contains a phenolic ring and organic carboxylic acid functionalities. Classes of naturally occurring phenolic acids are hydroxybenzoic acid and hydroxycinnamic acid, which are extensively found in nature, especially in vegetables, fruits and a variety of beverages like tea, coffee etc. The schematic diagram of phenolic acids and their application are summarised in Fig. 3A.1. Due to a wide variety of pharmacological activity and availability of hydroxycinnamic acids, the primary interest of researchers is to study the nature and dynamics for DNA-drug binding, which can lead to the design and construction of new and more efficient drugs targeted to DNA.

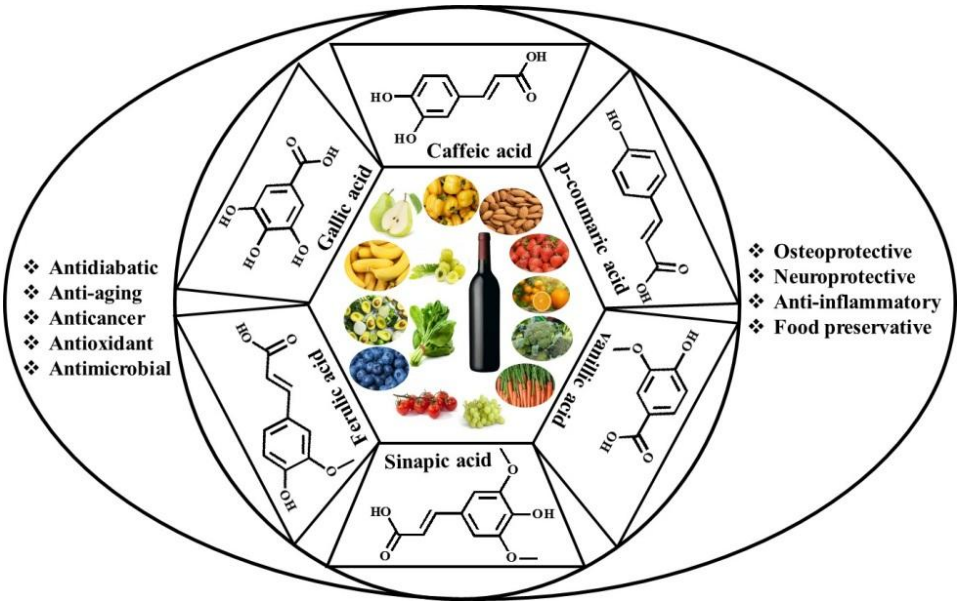

Figure 3A.1. Schematic diagram of different applications of phenolic acids

Generally, interaction of small molecules with calf thymus DNA (ct-DNA) occurs via three different binding modes such as intercalation, groove binding, and ionic interactions. In groove binding, the interaction of small molecules occur along the outside of the deep major groove or the shallow minor groove of the ct-DNA helix involving hydrogen bonding and van der Waals interaction; whereas for intercalation type of binding, small molecule inserts within the stacked planar base pair of native ct-DNA and in case of ionic interactions the interaction occurs between the negatively charged nucleic sugar-phosphate backbone and the positive or cationic ends of the small molecules [Guharay et al., 1997; Aramesh-Boroujeniet al., 2016; Ghoshet al., 2014].

Very few researchers have investigated the interaction of DNA with hydroxycinnamic acids and its derivatives. The interaction of caffeic acid with ct-DNA was investigated by Sarwar et al. and they concluded that caffeic acid interacted with ct-DNA through groove binding [Sarwaret al., 2017]. Zhang et al. investigated the interaction of ferulic acid with calf thymus DNA and according to them; ferulic acid binds to ct-DNA through intercalative mode [Zhang et al., 2013]. Another group of researchers investigated the interaction of chlorogenic acid with DNA at graphene modified electrode by cyclic voltammetry (CV). They found that the interaction between chlorogenic acid with DNA occurred through intercalative mode [Ma et al., 2016]. The interaction of functionalized gold and silver nanoparticles of chlorogenic acid with ct-DNA was investigated by Thomas et al. and they established that both silver and gold nanoparticles of chlorogenic acid bind through groove position of ct-DNA. They also observed that gold-coated nanoparticle of chlorogenic acid showed comparatively low cytotoxicity than its silver nanoparticle on normal human cell lines [Thomas at al., 2019]. So the observations of different groups have been found to be different in different cases.

Sinapic acid (SA) is one of the derivatives of hydroxycinnamic acid which has enormous biological activities such as anti-inflammatory, anti-oxidant, anti-bacterial, anti-cancer, anti-anxiety etc. [Kumar et al., 2019; Zou et al., 2002; Yoon et al., 2007; Yun et al., 2008]. Due to such activities of SA, it is well utilized in food, cosmetics, and pharmaceutical industries [Yun et al., 2008; Sengupta et al 2018; Lu et al., 2001; Nayab et al., 2016; Hameed et al., 2016]. However, to the best of our knowledge, no such literature is available about the nature of the interaction between SA and ct-DNA. In this context, to understand the therapeutic efficacy of SA on a molecular basis, it is important to acquire knowledge of its binding mode with appropriate biological targets, particularly proteins and DNA [Shyamala

et al., 2004; Guharay et al., 1997; Chaudhuri et al., 2007: Sengupta et al., 2019].

The present chapter demonstrates the binding interaction of SA with ct-DNA using spectroscopic and theoretical techniques to characterize their binding mode. UV-Vis spectroscopy, steady-state fluorescence spectroscopy, comparative ligand binding by the use of the well-known intercalator ethidium bromide, circular dichroism, DNA helix melting study, viscosity study, iodide quenching etc. have been utilized for this purpose [Jana et al., 2012;Sarkar et al., 2007]. All the experimental findings clearly established that SA resides in the groove position of DNA double helix. In addition, a theoretical study has also been carried out to visualize the actual docked position of SA in ct-DNA.

3A.2.Chemicals and Reagents

Calf thymus DNA (ct-DNA), ethidium bromide (EtBr) was purchased from SRL, India. Sinapic acid (SA) was supplied by Sigma Aldrich, USA. All other chemicals used were of HPLC grade and used without further purification.

3A.2.1. Preparation of Tris-HCl buffer stock solution

Tris, or tris(hydroxymethyl)aminomethane, (Molecular formula: $(HOCH_2)_3CNH_2$ and molecular weight: 121.14 g/mol). To prepare 1000 ml 1 M Tris-HCl buffer, at first we take 121.14 gm Tris in 800 ml triple distilled water. The pH was adjusted to 7.4 with addition of appropriate volume of concentrated HCl, finally volume was adjusted to 1000 ml by adding requisite amount of triple distilled water.

3A.2.2. Preparation of ct-DNA solution

The stock solution of ct-DNA was prepared in 0.01 M Tris-HCl buffer of pH 7.4 overnight at 4 °C. The concentration of ct-DNA was determined using absorption spectroscopy (ε_{260} =6600 L mol^{-1} cm^{-1}) [Zhou et al., 2015] and the purity of ct-DNA solution was measured by taking the absorbance ratio A_{260}/A_{280} which was in the range of 1.8-1.9 indicating the DNA was free from protein and pure for experimental use [Gangulyet al., 2015]. The stock solution was stored at -20 °C for further use. 5 mM standard stock solution of SA was prepared by dissolving in 1:4 alcohol/ Tris-HCl buffer medium.

3A.3. Instruments

3A.3.1. Absorption spectroscopy

UV-vis spectroscopic measurement was performed on a Hitachi U-2910 UV-spectrophotometer at 298K using a cuvette of 1.0 cm x 1.0 cm path length. Both SA and SA-ct DNA complexes were recorded in the wavelength range of 230-500 nm. A fixed amount of SA (10 µM) dissolved in the Tris-HCl buffer solution was used in sample cuvette and the absorption spectrum was monitored by the gradual addition of ct-DNA (0-120 µM) into both samples as well as reference cuvette in order to avoid any spectral interference from ct-DNA.

3A.3.2. Fluorescence spectroscopy

Steady-state fluorescence measurement was recorded on a Cary Eclipse fluorescence spectrophotometer (model G9800A) using 1.0 cm quartz cells. Fluorescence emission spectra of free SA and SA-ct-DNA were recorded in the range of 320-570 nm after excitation at 306 nm. The excitation and emission bandwidths were set at 10 nm and 5nm respectively. The titration was carried out by taking the fixed concentration of SA (25 µM) with increasing concentration of ct-DNA (0-950 µM) at three different temperatures (298, 303 and 308 K) and allowed to stand for 5 min to equilibrate before starting each temperature study experiment.

3A.3.3. Iodide quenching study

Iodide quenching experiments were performed on the same fluorescence spectrophotometer as described above. The quenching study was investigated by adding KI (0-170 mM) solution into SA (30 µM) and SA (30 µM)-ctDNA (60 µM) complex solution to measure the fluorescence intensity. The quenching constants (K_{SV}) in free and ct-DNA bound SA were calculated and then compared to analyze the interaction mode of SA and ct-DNA.

3A.3.4. Competitive displacement assay

A competitive displacement assay was conducted using the well-known intercalating probe ethidium bromide (EB). In this assay, a solution containing a fixed amount of ct-DNA (75 µM) and EB (25 µM) was titrated against the increasing concentration of SA (0-240 µM). The EB-ctDNA complex was excited at 480 nm and the emission spectra were recorded from 490-800 nm.

3A.3.5. DNA melting experiment

The DNA melting experiment was performed by taking the UV absorbance at 260 nm of pure ct-DNA (25 μM) and SA (40 μM)-ctDNA (25 μM) complex by varying the temperature from 35 to 90 °C. The denaturation temperature (T_m) of free ct-DNA and SA-ctDNA complex was determined from the midpoints of the curve based on $f_{ss}= (A-A_0)/(A_f-A_0)$ versus temperature (T) plot, where A_0 and A_f are the initial and final absorbance intensities respectively, and A is the absorbance intensity corresponding to its temperature [Zhou et al., 2015].

3A.3.6. Viscosity measurement

To get further evidence of the binding pattern of SA and ct-DNA a viscometric measurement was carried out by Ostwald viscometer. The viscometer was suspended in the water bath at 30 °C and SA concentration was increased (0 μM, 5 μM, 10 μM, 15 μM, 20 μM, 25 μM) with a fixed ct-DNA concentration (50 μM). A volume of 10 ml for each solution was considered for this experiment. Flow time was measured by a digital stopwatch, and the mean values were taken by replicated measurements of thrice to evaluate the viscosity of free ct-DNA and SA-ctDNA complex in a different molar ratio of SA to ct-DNA ([SA]/[ct-DNA]). The obtained data were plotted as $(\eta/\eta_0)^{1/3}$ against the ratio of [SA]/[ct-DNA], where η and η_0 are the viscosity of free ct-DNA and SA-ctDNA complex respectively.

3A.3.7. Circular dichroism spectroscopy

The circular dichroism (CD) spectra of ct-DNA were monitored in absence and presence of different amounts of SA at room temperature on a JASCO J-815 CD spectrometer with a scan speed of 120 nm per min and the wavelength ranges from 210 nm to 350 nm using a rectangular quartz cuvette of the path length of 1 cm. The concentration of ct-DNA was taken as 50 μM and molar ratios of [ct-DNA]/[SA] was 1:0, 1:0.5, 1:1. Each spectrum was an average of three collections of each data. The spectra of Tris-HCl buffer (10 mM, pH 7.4) was subtracted by taking the baseline correction.

3A.3.8. Steady-state fluorescence anisotropy measurement

Steady-state fluorescence anisotropy (r) measurements were performed on an F-7000 Hitachi spectro-fluorimeter equipped with a 1.0 cm path-length of rectangular quartz cell and a pair of polariser was used with excitation and emission wavelengths set to 306 nm and 427 nm respectively. The excitation and emission bandwidths were set as 10 nm and 5 nm

respectively. The steady-state anisotropy (r) was calculated by the following equations [Banerjee et al., 2012]:

$$r = (I_{VV} - G \times I_{VH}) / (I_{VV} + 2G \times I_{VH}) \quad (3A.1)$$

$$G = I_{HV} / I_{HH} \quad (3A.2)$$

where, I is the fluorescence emission intensity and the suffix VV denotes both the excitation and emission polarizers to be vertically aligned and VH indicates a vertically aligned excitation polarizer and horizontally aligned emission polarizer, HV corresponds to horizontally polarized excitation and vertically polarized excitation and so on. G is the correction factor. Titrations were carried out by various concentrations of ct-DNA ranging from 0-200 µM with a fixed concentration of SA (30µM) solution.

3A.3.9. Agarose gel electrophoresis

The gel electrophoresis experiment was performed according to Kasina Manojkumar et.al. with some modification [Manojkumar et al., 2015]. 10 µl of reaction mixture containing 2 µl of 3 µg/ml ct-DNA and 25, 50, 75 and 100 µM of SA solution were mixed and exposed to UVB (290-320 nm) radiation for 20 min. 2 µl of loading dye (Bromophenol blue) was then added and the rest was DEPC water prior to electrophoresis at 100 V for 1 h, at 25°C in a 0.8% agarose gel with 1X TAE buffer. After electrophoresis, the gel was stained with ethidium bromide at a concentration of 0.5µg/ml and photographed under UV light (BIO-RAD, ChemiDoc MP, Image system instrument).

3A.4. Software information: Theoretical studies (Molecular docking)

The crystal structure of DNA was obtained from the Protein Data Bank (PDB). The accession number of the crystal structure is 453D. Sinapate structure was also obtained from PDB (accession number 5XX). DNA and sinapate structures were prepared for docking in AutoDockTools using a previously published protocol [Ghosh et al., 2018]. Docking was performed with AutoDock 4.2 as well as AutoDockVina [Morris et al., 2009; Trott et al., 2010]. The whole DNA structure was placed in a parallelepiped grid box with dimensions of 25x25x45 $Å^3$. Gridpoint spacing was 0.375Å for AutoDock 4.2 and 1Å for AutoDockVina. Two lowest energy conformers were chosen for molecular dynamics (MD) simulation. MD was performed by Desmond [Bowers et al., 2006] as implemented in Schrödinger Maestro molecular modeling environment (Academic release 2018-1) following previously

published protocol [Pal et al., 2016]. OPLS_2005 all atom force field (Optimized potentials for liquid simulation) was used for the simulation. The ensemble type of the simulation was NPT with a constant number of molecules (N), a defined temperature T (298K) and pressure P (1 bar). Nose-Hoover thermostat and Martyna-Tobias-Klein barostat were used to maintain the temperature and pressure of the system, respectively [Bowers et al., 2006]. The complexes were placed in a simulation box maintaining a minimum distance of 10 angstrom from the periodic boundary such that the molecules do not interact with its periodic image. The system was minimized using the default relaxation protocol before simulation. The production MD was run for 4.8 ns.

3A.5. DNA binding studies

3A.5.1. UV-Vis absorption spectroscopy

Absorption spectroscopy is a simplest and most effective method to understand the ground-state interaction of small molecules (here, SA) and DNA [Zhou et al., 2015]. SA exhibited two absorption peaks at ~226 nm and ~306 nm for π-π^* and n-π^* transitions respectively, whereas, ct-DNA displayed maximum absorption at ~260 nm [Sengupta et al., 2018]. To obtain the binding interaction we have taken a calculated amount of SA (10 µM) in sample cuvette and ct-DNA (0-120 µM) was added to the solution cuvette as well as reference cuvette to avoid the any interference from the ct-DNA. The effect of the addition of ct-DNA on the absorption spectra of SA has been portrayed in Fig. 3A.2. According to the literature, intercalation binding between a small molecule and ct-DNA result in a hypochromic effect in the absorption spectra with a significant shift; whereas for weak interaction such as hydrogen bonding, groove binding and electrostatic interaction results no significant shift of the absorption maxima [Zhou et al., 2015]. Fig. 3A.2 (A) displayed a hypochromic effect without any significant shift at ~306 nm and ~226 nm. This observation suggested a weak interaction between SA and ct-DNA. Thus, to further quantify the appropriate binding mode of SA to ct-DNA we have performed the following experiments.

We have also determined the binding constant between ct-DNA and SA from the absorption titration data. The binding constant between SA and ct-DNA was calculated at the wavelength of 306 nm using the following equation [Zhang et al., 2013]:

$$\frac{1}{(A_0 - A)} = \frac{1}{A_0} + \frac{1}{KA_0[DNA]} \qquad (3A.3)$$

where A_0 and A are the absorbance of SA in the absence and presences of ct-DNA, respectively. K is the binding constant between SA and ct-DNA and [DNA] is the concentration of ct-DNA. The plot of $1/(A_0-A)$ versus the reciprocal value of the ct-DNA concentration was found to be linear, with a slope equal to the value of $1/KA_0$. The value of K can be calculated using the intercept, $1/A_0$ and slope, $1/KA_0$. The double reciprocal plot of $1/(A_0-A)$ versus 1/[DNA] at 298K has shown in Fig. 3A.2(B). The calculated binding constant is 4.68 x 10^3 M^{-1}. The lower K value indicated that there is a weak interaction between SA and ct-DNA. It has already been reported that the binding constant of probes to DNA by intercalation mode usually lies in the range of 10^4-10^6 M^{-1}. According to the available literature, the binding constant values of acridine orange [Arndt-Jovin et al., 1989; Darzynkiewicz et al., 1990] and EB [Lepecq et al., 1967], classical intercalating agents being 3.1 x 10^4 and 4.3 x10^5 M^{-1}, respectively. These results indicated that the binding mode of SA and ct-DNA may be a groove binding mode.

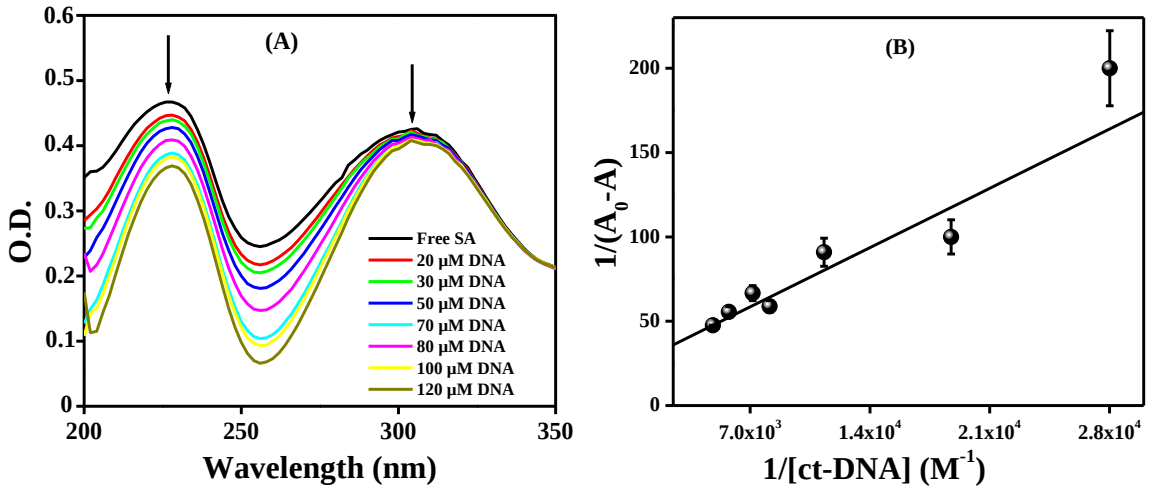

Figure 3A.2. Figure (A) represents the absorption spectra of SA (10 µM) with an increasing concentration of ct-DNA (0-120 µM). Figure (B) represents the double reciprocal plot of ct-DNA with SA

3A.5.2. Steady-state fluorescence spectroscopy

The fluorescence emission spectrum of SA exhibits emission maximum at ~430 nm when excited with a wavelength of 306 nm. Upon the addition of ct-DNA, a gradual decrease in the emission intensity was observed with no apparent shift (vide Fig. 3A.3(A)). The quenching of intrinsic fluorescence intensity of SA in the presence of ct-DNA indicated a complex

formation [Sengupta et al., 2018]. To ascertain the quenching mechanism, the following Stern-Volmer equation was employed (equation 3A.4): [Lakowicz, 2006]

$$\frac{F_0}{F} = 1 + K_{SV}[Q] = 1 + k_q\langle\tau_0\rangle[Q] \qquad (3A.4)$$

where F_0 and F are the fluorescence intensities of SA in the absence and presence of ct-DNA (quencher), respectively, and [Q] is the concentration of ct-DNA. K_{SV} is the Stern-Volmer quenching constant which can be evaluated from the linear relation of F_0/F and [Q]. k_q is the bimolecular quenching rate constant, and $\langle\tau_0\rangle$, the average fluorophore lifetime in the absence of quencher compounds is the order of 10^{-9} s. In general, fluorescence quenching can occur via static quenching (ground-state complex formation) or dynamic quenching (collisional quenching). The presence of static or dynamic quenching can be well recognized by performing a temperature variation experiment and evaluating K_{SV} values at different temperatures. The plot of F_0/F vs. different concentrations of [ct-DNA] at three different temperatures has been displayed in Fig. 3A.3(B) and the corresponding K_{SV} values are accumulated in Table 3A.1. Also using the K_{SV} values the bimolecular quenching constant (k_q) at three temperatures are found to be the order of ca. 10^{11} $M^{-1}s^{-1}$ (Table 3A.1).

As evident from table 3A.1, a steady increase of K_{SV} values with increasing temperature convincingly suggested the presence of dynamic quenching in the operative quenching mechanism. For dynamic quenching mechanism the maximum threshold collision quenching constant is $2x10^{10}$ $M^{-1}s^{-1}$ [Lakowicz, 2006]. As we can see from table 3A.1, k_q values are somewhat higher than the diffusion controlled quenching constants supporting the occurring of static quenching process. Furthermore, the distinction between the static and dynamic quenching process could be envisaged from the UV-Vis spectra of the fluorophore-quencher complexes. Gradual addition of quencher to the fluorophore results in the slight change in the absorption spectra with the hypsochromic shift of the peak again confirmed the static quenching process to be predominantly operating in the complex formation between SA and ct-DNA (Fig. 3A.2(A)). Generally, in case of static quenching the quenching efficiency of the fluorophore in the binding interaction should decrease with increasing temperature as a destabilization process occurring in the ground state complex formation between the fluorophore and quencher [Lakowicz, 2006].

In the contrary, we observed the opposite situation for the interaction of SA with ct-DNA interaction. One attempt can be taken to explain this anomalous situation by Arrhenius theory [Tian et al., 2010; Ghosh et al., 2015]. According to Arrhenius equation

$$\ln k_q = \ln (K_{sv}/\langle\tau_0\rangle) = -E_a/RT + \ln A \qquad (3A.5)$$

where, A is the pre-exponential factor. E_a is the activation energy for the quenching process. The rate constant (k) i.e. the bimolecular quenching constant (k_q) for the quenching process depends on temperature. Higher the temperature, higher will be the rate constant value. At higher temperature, the increase in the bimolecular quenching constant value outweigh the decrease the k_q value due to destabilization of the complexes with increase in temperature [Tian et al., 2010; Ghosh et al., 2015]. Considering the linear plot of ln k_q vs. 1/T, the activation energy was found to be 14.83 kJ mol^{-1} [inset of Fig. 3A.3(B)]. The value is somewhat higher as compared to the other biomolecular reactions [Tian et al., 2010; Ghosh et al., 2015], clearly enlighten the considerable effect of the temperature on the fluorescence quenching occurring via static quenching process in the interaction of SA with ct-DNA.

The static quenching process could be understood through the modified Stern-Volmer Equation [Lakowicz, 2006; Han et al., 2009; Lehrer, 1971].

$$\frac{F_0}{\Delta F} = \frac{F_0}{(F_0 - F)} = \frac{1}{f_a K_a}\frac{1}{[Q]} + \frac{1}{f_a} \qquad (3A.6)$$

where, f_a represents the fraction of accessible fluorescence and K_a is the modified Stern-Volmer quenching constant. The plot of $F_0/\Delta F$ vs. 1/[Q] is linear with slope ($1/ f_aK_a$) and intercept is ($1/f_a$). Fig. 3A.3(C) represents the modified Stern-Volmer plots for the interaction of SA with ct-DNA at three different temperatures and modified Stern-Volmer quenching constant (K_a) values in each case are tabulated in table 3A.1. The modified Stern-Volmer quenching constant values were also found to vary appreciably with temperature which supported the static quenching mechanism.

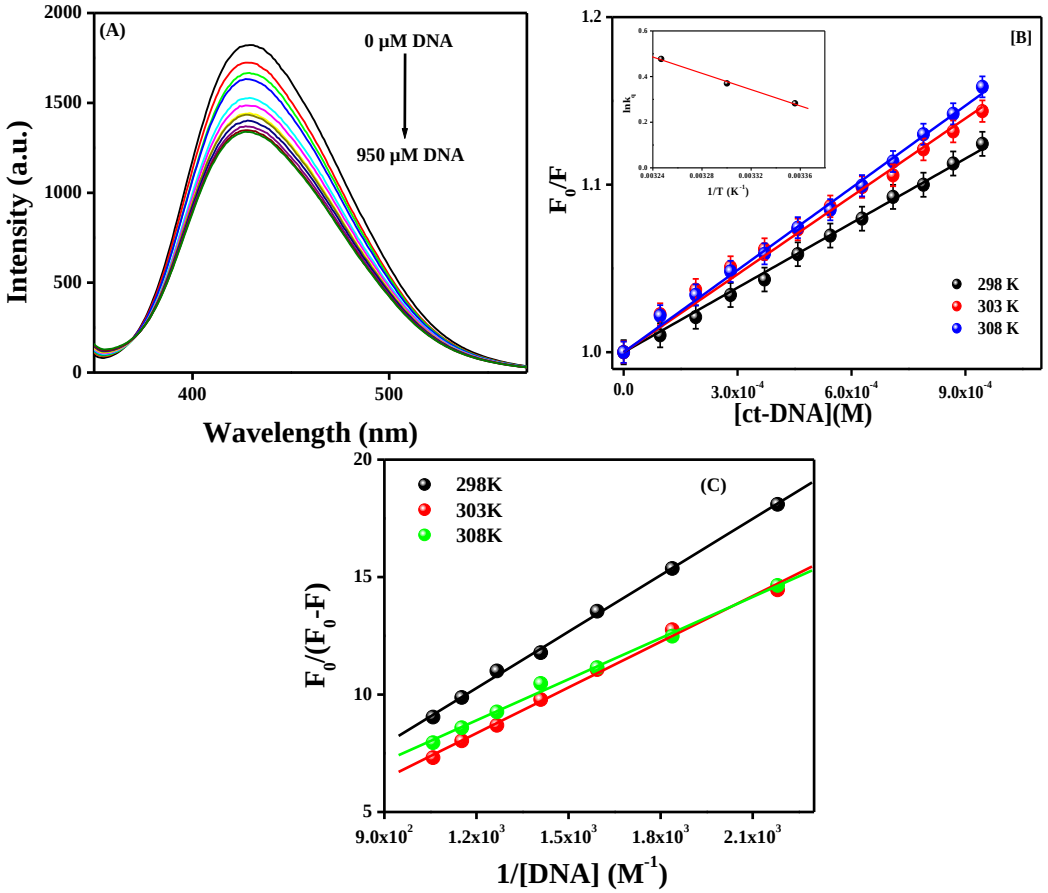

Figure 3A.3. Fluorescence quenching spectra of 30 µM SA (——) with varying concentration of ct-DNA (0-950 µM) at room temperature (A) and Stern-Volmer plots of SA with ct-DNA at three different temperatures (B). Inset: Arrhenius plots for the fluorescence quenching of SA with the addition of ct-DNA at different temperatures. Modified Stern-Volmer plots for the interaction of SA with ct-DNA at three different temperatures (C)

Table 3A.1. Variation of Stern-Volmer quenching constant (K_{SV}) and bimolecular quenching constant (k_q) and modified Stern-Volmer quenching constant at three different temperatures for SA-ct-DNA system

T (K)	K_{SV} (M^{-1})	R^2	k_q($M^{-1}s^{-1}$)	K_a (M^{-1})
298	132.69	0.998	1.327x 10^{11}	0.823x10^2
303	144.83	0.996	1.448x10^{11}	0.870x10^2
308	161.21	0.996	1.612x10^{11}	3.23x10^2

3A.5.3. Evaluation of binding constant and thermodynamic parameters

The values of binding constant (K_b) at three different temperatures can be evaluated by using fluorescence data. The following equation was employed to calculate the K_b values (equation 3A.7) [Lakowicz, 2006]:

$$\log\frac{(F_0 - F)}{F} = \log K_b + n\log[Q] \qquad (3A.7)$$

where, K_b and n are binding constant and the number of binding sites respectively. The value of K_b and n can be obtained from the intercept and slope of the plot log $[(F_0\text{-}F)/F]$ vs. log [Q]. The values of K_b and n are listed in Table 3A.2. A gradual decrease in K_b value with increasing temperature pointed towards the destabilization of the complex at a higher temperature (Fig. 3A.4(A)). A similar observation was also observed by Sarwar et al. and Thomas et al. Sarwar et al. worked with the interaction of caffeic acid with ct-DNA and Thomas et al. worked with both silver and gold nanoparticles of chlorogenic acid with ct-DNA. According to them the K_b values for the interaction of caffeic acid and gold nanoparticle of chlorogenic acid with ct-DNA was almost 13 and 17 times higher than that of our estimated value for SA-DNA interaction, respectively [Sarwar et al., 2017; Thomas et al., 2019]. The lower value of K_b could be explained due to the presence of two bulky methoxy groups in SA.

Thermodynamic parameters are crucial to predict the nature of interaction forces involved in the interaction of small molecules with DNA. Various types of interaction such as hydrogen bonding, hydrophobic forces, van der Waals forces, and electrostatic interactions can occur between SA and ct-DNA. According to Ross and Subramanian [Ross et al., 1981] the interactive forces can be classified as follows based on the values of entropy change (ΔS) and enthalpy change (ΔH):

ΔH<0, ΔS<0: van der Waals interaction and hydrogen bond formation.

ΔH>0, ΔS>0: hydrophobic interaction.

ΔH<0, ΔS>0: electrostatic interaction.

The values of free energy change (ΔG), entropy change (ΔS) and enthalpy change (ΔH) were analyzed using the following van't Hoff equation (equation 3A.8) [Ross et al., 1981]:

$$\ln K_b = -\frac{\Delta H}{RT} + \frac{\Delta S}{R} \qquad (3A.8)$$

$$\Delta G = \Delta H - T\Delta S \qquad (3A.9)$$

where R is the universal gas constant (8.314 kJ K^{-1} mol^{-1}) and T is the temperature (in Kelvin). The van't Hoff plot has been displayed in Fig. 3A.4(B) and 3A.4(C). ΔH and ΔS values have been determined from slope and intercept of $\ln K_b$ vs. 1/T plot respectively. The

results are summarized in Table 3A.2. It is evident that the values of both ΔH and ΔS are negative, corresponding to the presence of van der Waals interaction and hydrogen bond formation during complex formation of SA with ct-DNA. The negative sign for ΔG indicated the spontaneity of the binding process between SA and ct-DNA.

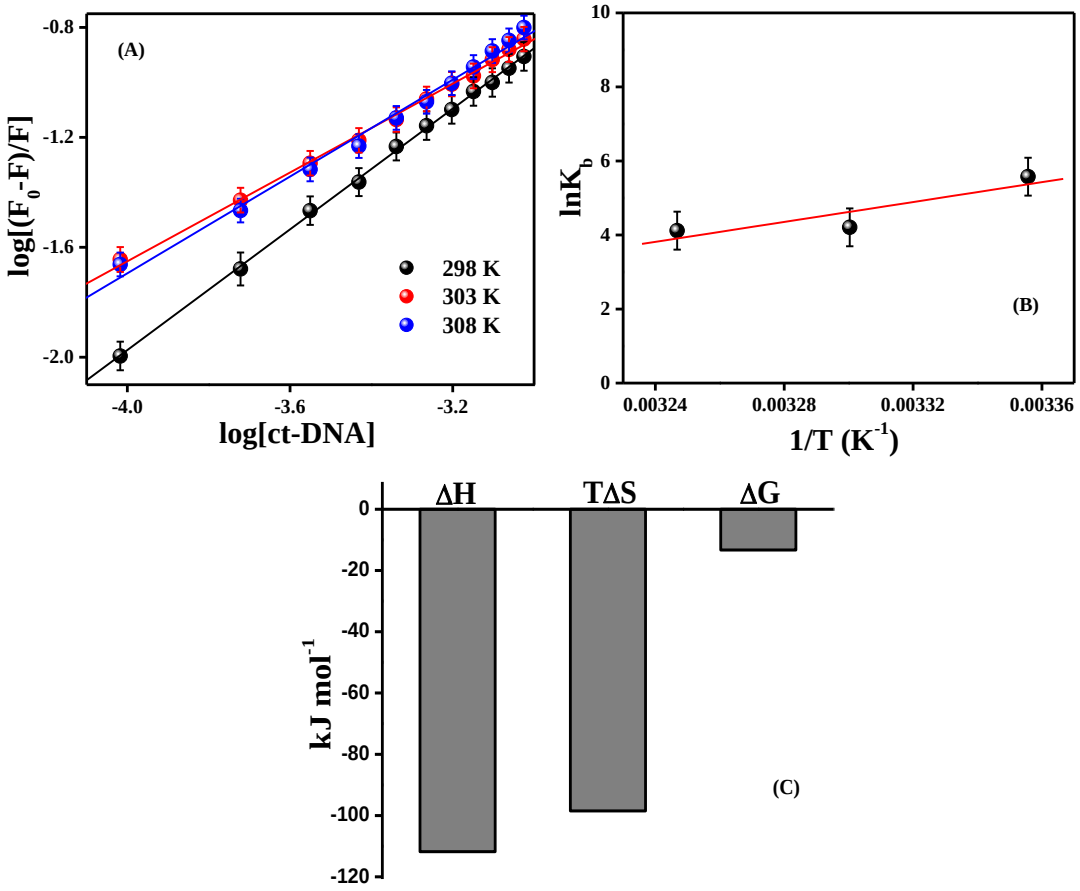

Figure 3A.4. The plot of log [(F_0-F)/F] vs log [Q] for SA-ctDNA complex at three different temperatures (A), van't Hoff plot at three different temperatures for binding of SA-ctDNA system (B) and bar diagram plot to visualize the thermodynamic parameters of SA and ct-DNA at 298 K (C)

Table 3A.2. Binding constant and other thermodynamic parameters at three different temperatures for SA-ctDNA system

T (K)	K_b (M^{-1})	n	R^2	ΔH (kJ mol^{-1})	ΔS (J mol^{-1})	ΔG (kJ mol^{-1})
298	263.8	1.09	0.998	-111.78	-330.46	-13.30
303	67.18	0.88	0.992			-11.65
308	37.92	0.81	0.996			-10.00

3A.5.4. Competitive displacement assay

Now to confirm the interaction pattern of SA with ct-DNA a competitive displacement assay experiment was conducted by the use of a well-known dye whose binding mode is already established.

Ethidium bromide (EB) is such a dye which binds to ct-DNA through intercalation [Zhou et al., 2015]. EB shows a weak fluorescence in solution; however, with the addition of ct-DNA, due to its intercalation, the fluorescence intensity increases remarkably. If SA binds to ct-DNA through the same binding mode as EB, the fluorescence intensity of EB-ctDNA complex should decrease because of the displacement of EB from the same binding site by SA [Rehman et al., 2014; Olmsted III et al., 1977]. The fluorescence spectra of the EB-ctDNA complex in the absence and presence of SA is shown in Fig. 3A.5. Fig. 3A.5 shows that the fluorescence intensity of EB-ctDNA does not quench significantly on subsequent addition in increasing amounts of SA. This result indicated that SA was unable to replace EB in the ct-DNA helix. Thus these results prove that SA binds to ct-DNA via non-intercalative binding mode.

However non intercalative binding includes electrostatic and groove binding. Since we have already discussed in the introduction that electrostatic binding involve interaction of a positively charged molecule with the negative backbone of DNA, hence its presence can be ruled out [Smyk et al., 1989].

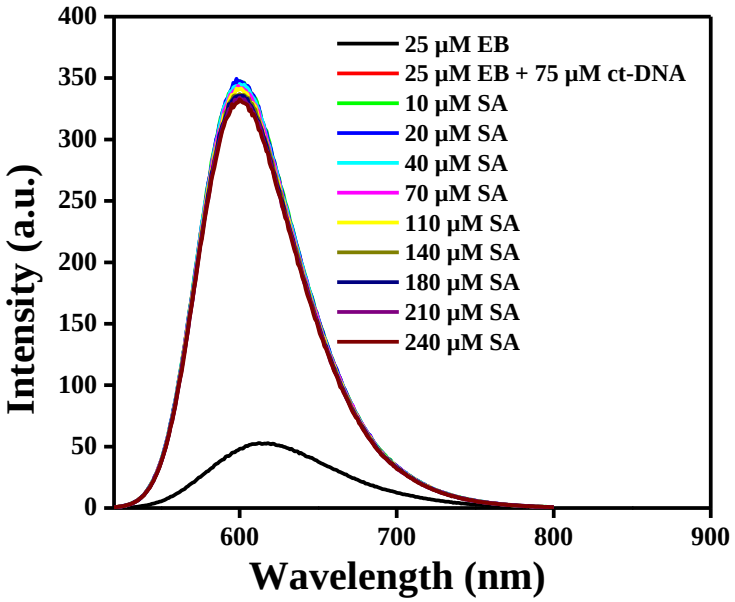

Figure 3A.5. Fluorescence emission spectra of native EB and EB-ctDNA complex with increasing concentration of SA (0-240 µM)

3A.5.5. Iodide quenching study

To support the groove binding mode of interaction between SA and ct-DNA, fluorescence quenching experiment was carried out with potassium iodide (quencher). Iodide ions (I^-) generally quench the fluorescence intensity of small molecules in the aqueous medium. DNA is also a negatively charged (due to the phosphate group) macromolecule which can repel the iodide ions. Thus if the small molecules intercalate into the double-stranded DNA then the small molecule is well protected from the ionic quenchers and hence their fluorescence intensity will not quench significantly [Ling et al., 2008]. While in the case of groove binding or electrostatic binding the small molecules are well exposed and hence fluorescence intensity of these molecules can be quenched significantly by gradual addition of I^- [Ling et al., 2008]. In our study, K_{SV} values for the interaction of SA-KI system in the absence and presence of ct-DNA was calculated from equation 3A.4 to observe the extent of fluorescence quenching (Fig. 3A.6). Table 3A.3 shows that in the absence and presence of ct-DNA, the values of K_{SV} was found to be 6.36 M^{-1} and 6.39 M^{-1} respectively. Therefore an insignificant reduction in the quenching efficiency ruled out any possibility of intercalative binding and indicated that the DNA bound probe is much more accessible to the ionic quencher. The lesser degree of reduction in the K_{SV} values can also be attributed to the external or groove binding mode between SA with DNA.

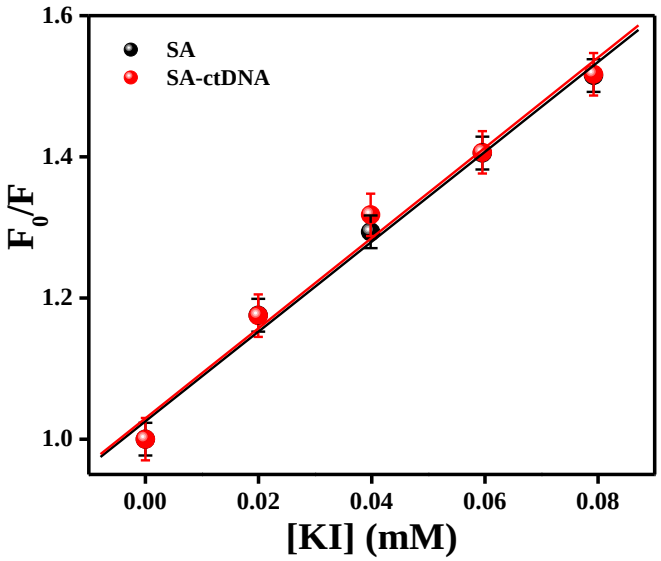

Figure 3A.6. Stern-Volmer quenching plot of SA (30 µM) by KI concentration in the absence and presence of ct-DNA

Table 3A.3. K_{SV} values obtained in KI quenching of SA in the absence and presence of ct-DNA

System	K_{SV} (M^{-1})	R^2	Change in K_{SV} (%)
SA	6.36	0.9949	-
SA + ct-DNA	6.39	0.9917	0.47

3A.5.6. DNA melting experiment studies

The hydrogen bonding and stacking interaction between the base pair of purine and pyrimidines stabilize the double helix of DNA. With increasing temperature, the stability of DNA double-strand decreases and goes to single strands. The thermal decomposition of DNA double helix is measured by its melting temperatures (T_m). Melting temperature is the temperature at which half of the DNA double helix is denatured to form single strands [Chaveerach et al., 2010]. When small molecules bind with ct-DNA through intercalation, the stability of DNA double helix increases which in turn enhances the melting temperature (5-8 °C) of DNA. For groove binding or electrostatic interaction, there is an insignificant amendment in melting temperature [Kumar et al., 1993]. The melting temperature of DNA helix is performed by measuring the absorbance at 260 nm as a function of temperature. In this case, we have monitored the change in T_m of ct-DNA in the absence and presence of SA. From the melting profile in Fig 3A.7, the calculated melting temperature values of ct-DNA and SA-ctDNA complex appeared at 66.2 °C and 67.4 °C respectively, obtained from the curves in Fig. 3A.7. Thus it was evident that the binding of SA does not lead to a significant increase in the T_m of ct-DNA. The small change in the T_m suggested the groove binding nature of SA with ct-DNA [Kumar et al., 1993].

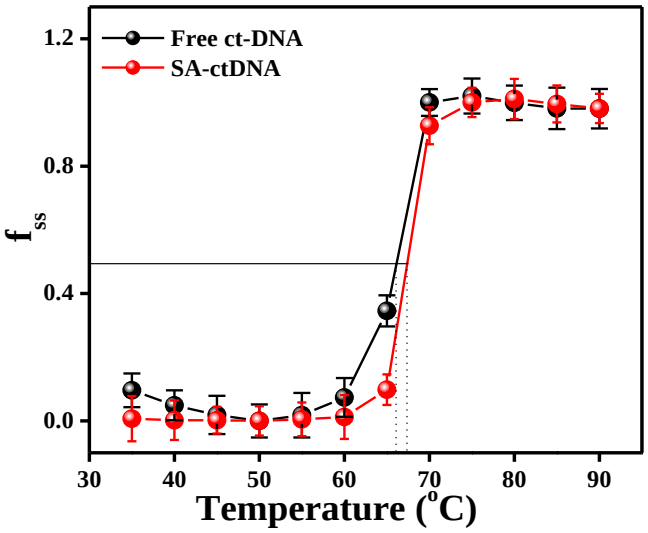

Figure 3A.7. Thermal decomposition curve of free ct-DNA and SA-ctDNA complex at pH 7.4. [ct-DNA]= 25 x 10^{-6} (M) and [SA]= 40 x 10^{-6} (M)

3A.5.7. Viscosity measurements

A viscosity measurement provides necessary and adequate information for the evaluation of mode of the binding interaction between small molecules and DNA. For an intercalative mode of binding the viscosity of DNA solution generally increases due to the lengthening of the DNA helix [Husain et al., 2013]. By contrast, non-intercalative binding could reduce the overall length of DNA hence there will be a minor or no change in the viscosity of DNA solution [Zhang et al., 2014]. To support this standpoint, a set of solutions were prepared which contained a fixed concentration of ct-DNA and various concentrations of SA. Then, the viscosity measurements were performed at room temperature. The results of this study are presented in the plot of $(\eta/\eta_0)^{1/3}$vs. [SA]/[ct-DNA] is shown in Fig. 3A.8. According to Fig. 3A.8, there is an insignificant variation of relative specific viscosity of ct-DNA in presence of SA. Such type of behavior illustrates that SA interacts via non-intercalative and preferentially groove binding mode of the probe.

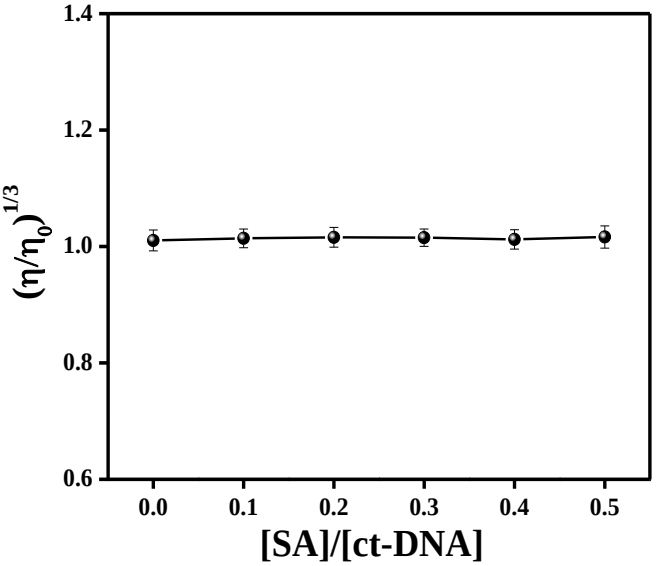

Figure 3A.8. Viscosity measurement plot of ct-DNA (50 μM) with increasing concentration of SA

3A.5.8. Circular dichroism (CD) studies

We have also deciphered the conformation change of DNA using circular dichroism technique during SA-DNA interaction. The CD-spectrum of DNA displayed a duplex, characterized by a negative band at 246 nm for right-handed helicity and a positive peak at 276 nm for base pair staking interaction of a canonical B-form conformation [Husain et al., 2013; Ranjbar et al., 2009; Basu et al., 2013]. For intercalative type binding of a small molecule with ct-DNA, both bands of DNA in the CD-spectra changes remarkably, while for groove or electrostatic binding with small molecules there is nominal impact on the CD-spectrum [Husain et al., 2013; Qaiset al., 2017]. Now to determine the change in DNA conformation in presence of SA, the intrinsic CD spectra of ct-DNA was recorded in presence of various concentration of SA. Fig. 3A.9 revealed both bands of the CD spectrum of ct-DNA did not change significantly with increasing concentration of SA. This indicated that the binding of the probe with ct-DNA did not disturb the stacking of the bases. Therefore the CD profile confirmed the binding mode of the fluorophore SA to the host DNA to occur through groove binding. However the negligible change in the CD profile may be due to the conformational changes from B-form to A-form [Qaiset al., 2017].

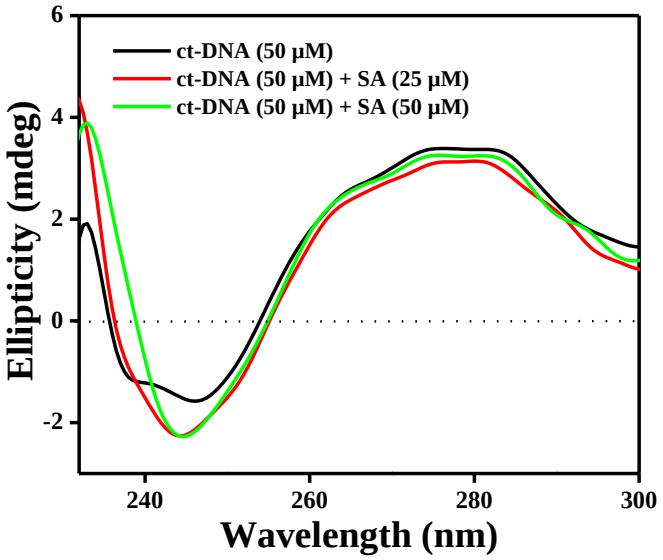

Figure 3A.9. Far-UV CD spectra of ct-DNA on the addition of varying concentration of SA

3A.5.9. Fluorescence anisotropy

The mobility of small molecule is greater in a less viscous solvent. But the mobility gets restricted when it gets bound with macromolecules like proteins, DNA, cyclodextrin, etc [Das et al., 2007; Bose et al., 2019]. Hence fluorescence anisotropy method is generally utilized to identify the changes in the microenvironment around a small fluorescent molecule with the addition of macromolecules. When DNA binds to the small molecule through intercalative mode the inflexibility increases around the small molecule hence the anisotropy increases because the small molecule inserts within the stacked planar base pair of native DNA. But for groove binding, the fluorescence anisotropy does not change at all [Chi et al., 2010; Wang et al., 2018; Modukuruet al., 2005]. Fig. 3A.10, exhibits the change of fluorescence anisotropy with gradual addition of ct-DNA to the SA solution. The anisotropy values were found to remain almost constant. This observation indicated that the flexibility of SA remained unaltered after binding to ct-DNA. Thus, we further concluded that binding of SA and ct-DNA was groove binding rather than the intercalative type.

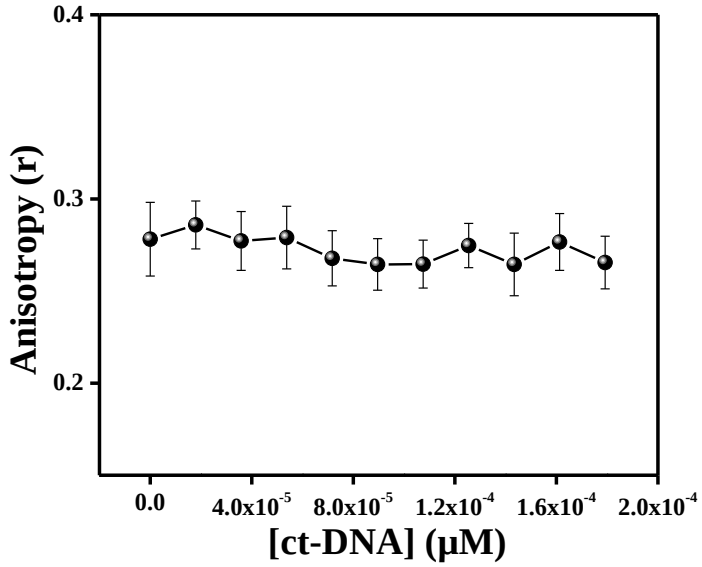

Figure 3A.10. Fluorescence anisotropy plot of SA (30 µM) and ct-DNA (0-2×10^{-4} M)

3A.5.10. Gel electrophoresis

To observe and assess the protecting activity of SA against UVB radiation induced DNA damage, we have monitored the agarose gel electrophoresis profiles of SA treated ct-DNA vs unbound ct-DNA on exposure to UVB radiation. The picture has been portrayed in Fig. 3A.11. As evident from lane 1, the normal ct-DNA (SA-UV-) exhibited an intense band. But as observed in lane 2, on exposure to UVB radiation the band intensity reduced, and the smear in the lane 2, representing the damaged/fragmented ct-DNA intensified [Georgiou et al., 2009]. In presence of SA (25 µM to 100 µM) [lane 3 to 6] the damaging effect of UVB radiation on ct-DNA appeared to be reduced, as evident from increase in band intensity and decrease in smear intensity compared to lane 2. Densitometric analysis using ImageJ-win64 software indicated that the ct-DNA band intensity as well as smear patterns in individual lanes of the agarose gelelectrophoresis profile further validated the protective activity of sinapic acid against UVB induced DNA damage (Fig. 3A.11. (A), (B), and (C)). Precisely 50 µM SA was found to have the maximum protective activity against UVB induced ct-DNA damage. However, for higher concentrations of sinapic acid, the protective activity decreases.

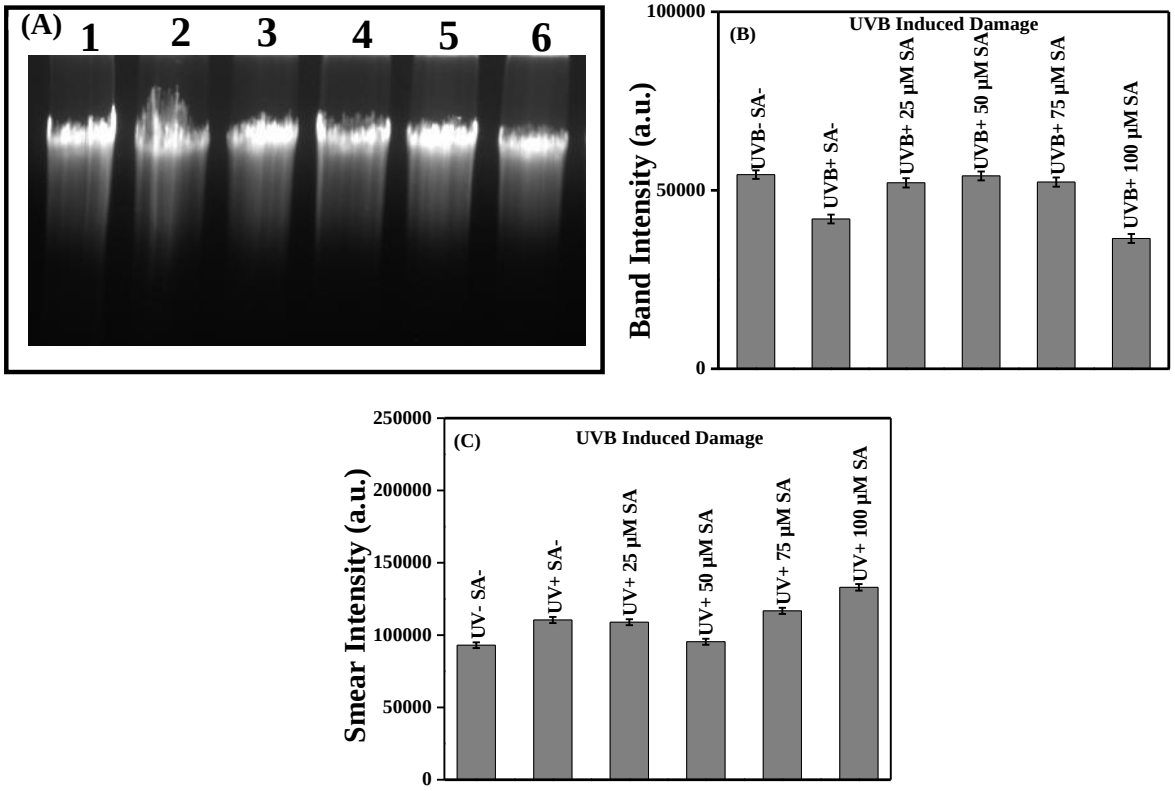

Figure 3A.11. Agarose gel electrophoretic pattern of ct-DNA in the absence and presence of varying concentrations of SA; Lane 1, free ct-DNA without UVB radiation; lane 2, free ct-DNA with UVB radiation; lane 3, ct-DNA+ 25 µM SA with UVB radiation; lane 4, ct-DNA+ 50 µM SA with UVB radiation; lane 5, ct-DNA+ 75 µM SA with UVB radiation; lane 6, ct-DNA+ 100 µM SA with UVB radiation. Where (A) corresponds to the image of the gel, (B) and (C) corresponds to agarose gel electrophoresis intensity plot of the band part and the smearish part recpectively

3A.5.11. Molecular docking

SA in pH 7.4 is reported to exist as anion [Han et al., 2009] so docking was performed with sinapate anion instead of neutral sinapic acid. Binding of sinapate ion with DNA was found to be energetically favourable. Lowest binding energy as obtained by docking was -24.14 kJ/mol (25.52 kJ/mol in AutoDockVina). Two most favourable binding conformations are shown in Fig. 3A.12. Sinapate ion was found to bind exclusively in the minor groove of DNA and specifically in the GC rich region. It can also form a hydrogen bonding interaction through its methoxy group with the $-NH_2$ group of guanine base (Fig. 3A.13(A)). Donor acceptor distance was found to be 2.9 Å. MD simulation showed stable interaction of sinapate with DNA for about 2.5 ns, after which sinapate dissociated from

DNA (Fig. 3A.13(A)). Both the Coulombic and van der Waals interactions were observed between sinapate and DNA, however, the van der Waals force was found to be the major contributing force (Fig. 3A.13(B)). sinapate ion formed H bond with DNA for the whole duration during which it remained bound to DNA (Fig. 3A.13(B)). Distances from three nearby guanine bases were computed over the simulation trajectory to study the fluctuations of SA in the binding site (Fig. 3A.13(C)) of DNA. It was found that while bound sinapate ion remained very stable in the minor groove of DNA. Dissociation of sinapate ion from DNA after ~2.5 ns during MD simulation suggested a low binding affinity constant, which corroborated with the experimental observation (cf Table 3A.1). After a series of spectroscopic experiments, molecular docking was employed to have a better understanding of our data. The similar nature of groove binding was also found for the interaction of silver/gold functionalized nanoparticles of chlorogenic acid, and caffeic acid with ct-DNA [Thomas et al., 2019; Sarwar et al., 2017].

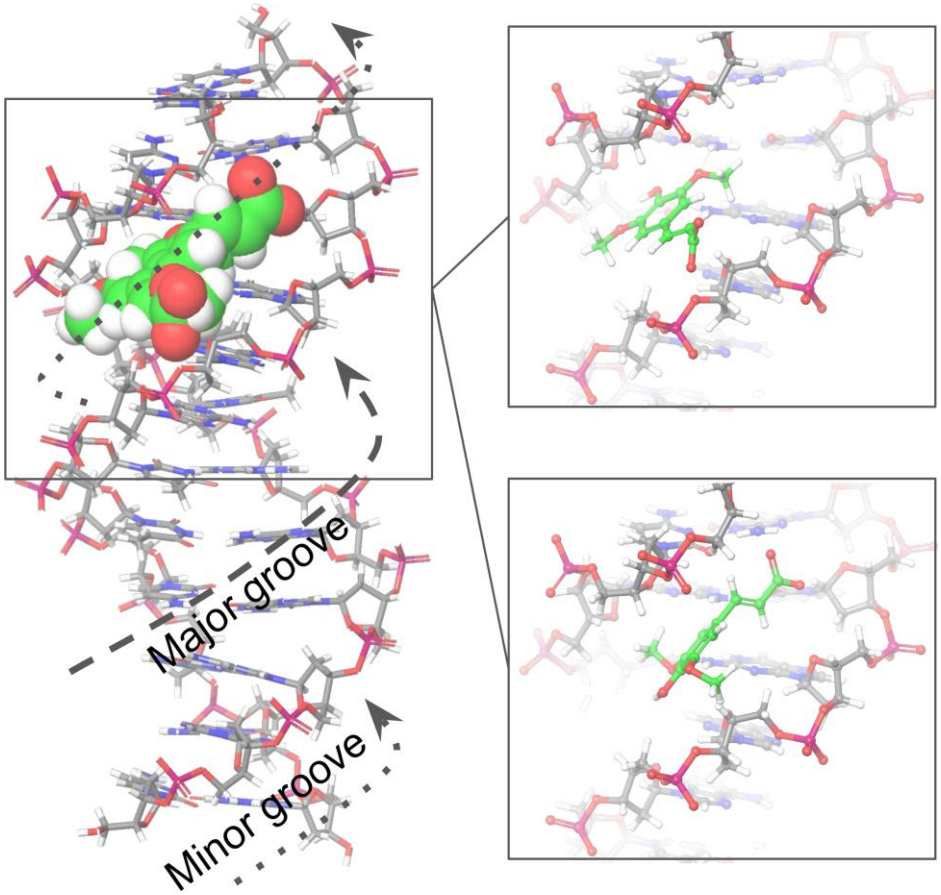

Figure 3A.12. Binding of sinapate (green) in the minor groove of DNA as obtained by molecular docking simulation. Two possible binding conformations are shown superimposed and separately

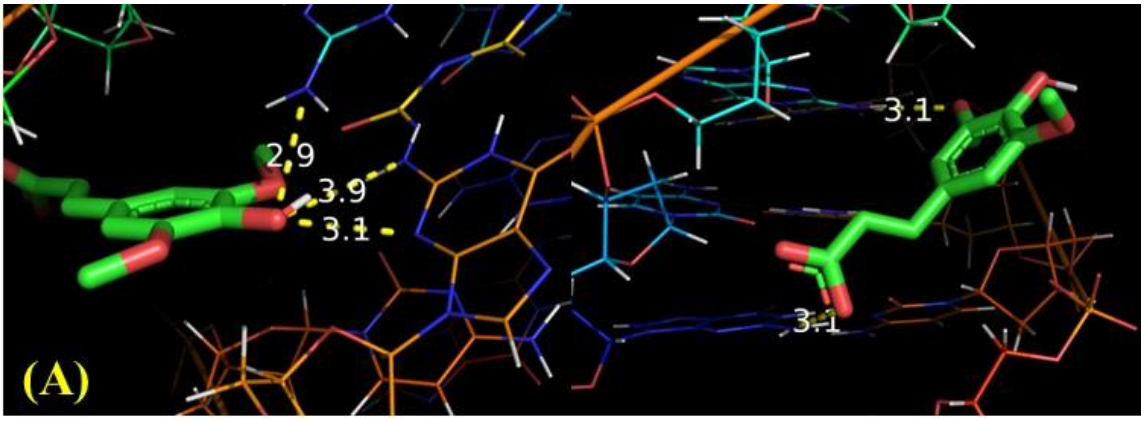
2.9
3.9
3.1
3.1
3.1
(A)

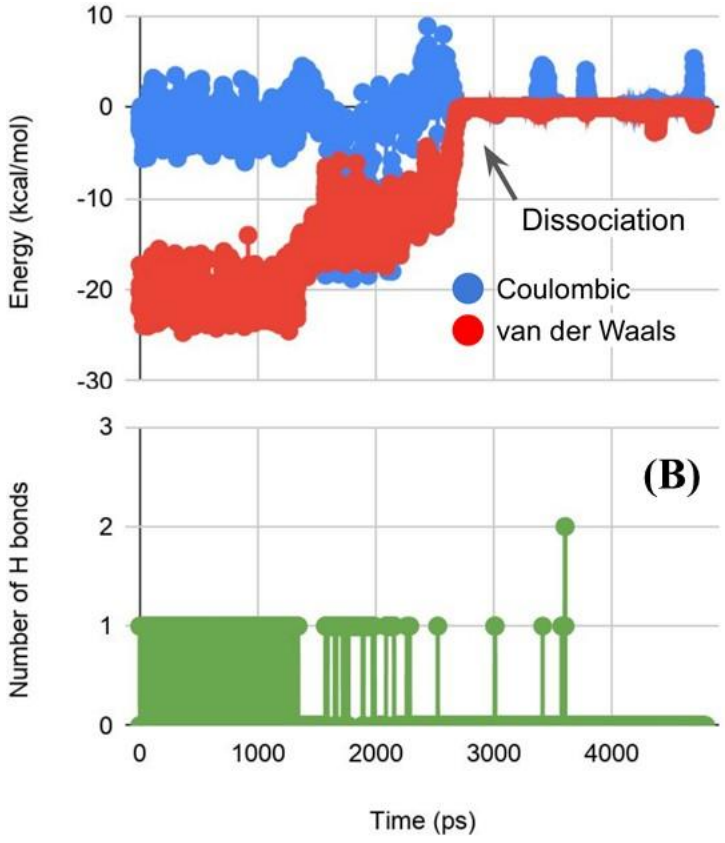
Energy (kcal/mol)
10
0
-10
-20
-30
Dissociation
Coulombic
van der Waals
Number of H bonds
3
2
1
0
(B)
0
1000
2000
3000
4000
Time (ps)

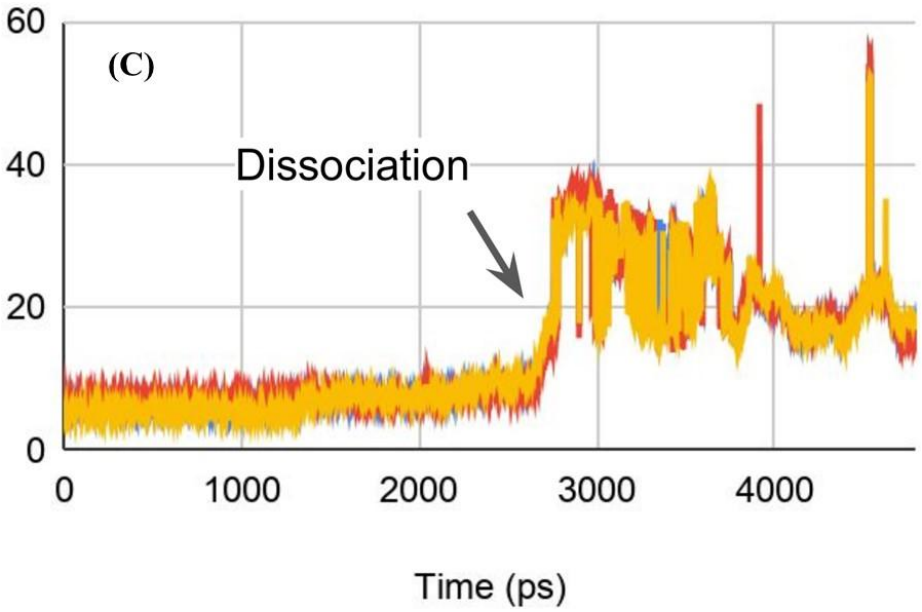

Figure 3A.13. (A): Hydrogen bonds between SA and the bases of DNA as obtained from molecular docking. Donor acceptor distances are shown. Two most favourable binding conformations of SA are shown. (B): Binding energy of SA with DNA and the H bonding over the period of simulation. Point of dissociation of SA from DNA is marked with an arrow. (C): Distance between C1 of SA and the -NH_2 group of three adjacent three guanine bases viz. G10 of chain A (blue) G14 of chain B (red) and G16 of Chain B (yellow). Point of dissociation of SA from DNA is marked

3A.6. Conclusion

The present chapter provides a clear indication of the binding interaction of SA with ct-DNA. The quenching of fluorescence intensity of SA confirmed that the quenching mechanism was a static quenching type. The binding constants and the number of binding sites were calculated at three different temperatures. Various thermodynamic parameters were calculated which suggested that the binding process was spontaneous and involvement of hydrogen bonding and weak van der Waals forces of interaction between the probe and ct-DNA are responsible for the groove binding of this particular polyphenol with the bio macromolecule. Gel electrophoresis result clearly indicated that SA can protect the DNA damage from UVB radiation. The molecular docking and molecular dynamics further confirmed that the SA binds to DNA via minor groove with a binding energy of ~-5.769 kcal mol^{-1} and also conform to the spectroscopic results. Additionally, we have compared our findings with other reported hydroxycinnamic acid derivatives to get an idea about the

structure-activity relationship. In our view, the presence of bulky methoxy groups in SA affected its binding affinity with DNA. Finally, in the view of biological research, this report has successfully enlarged the scope for using SA as a drug and DNA binder with further scope for development. In addition, the work will encourage further development of SA analogous compounds in future for relevant pharmacological applications.

3A.7. References

Aramesh-Boroujeni, Z., Khorasani-Motlagh, M., Noroozifar, M., 2016. Multispectroscopic DNA-binding studies of a terbium (III) complex containing 2, 2′-bipyridine ligand. Journal of Biomolecular Structure and Dynamics. 34, 414-426.

Arndt-Jovin, D.J., Jovin, T.M., 1989. Fluorescence labeling and microscopy of DNA. Methods in Cell Biology. 30, 417-448.

Banerjee, M., Pal, U., Subudhhi, A., Chakrabarti, A., Basu, S., 2012. Interaction of Merocyanine 540 with serum albumins: photophysical and binding studies. Journal of Photochemistry and Photobiology B: Biology. 108, 23-33.

Basu, A., Kumar, G.S., 2013. Biophysical studies on curcumin-deoxyribonucleic acid interaction: spectroscopic and calorimetric approach. International Journal of Biological Macromolecules. 62, 257-264.

Bose, A., Sengupta, P., Pal, U., Senapati, S., Ahsan, M., Roy, S., Das, U., Sen, K., 2019. Encapsulation of Thymol in cyclodextrin nano-cavities: A multi spectroscopic and theoretical study. Spectrochimica Acta Part A: Molecular and Biomolecular Spectroscopy. 208, 339-348.

Bowers, K.J., Chow, E., Xu, H., Dror, R.O., Eastwood, M.P., Gregersen, B.A., Klepeis, J.L., Kolossvary, I., Moraes, M.A., Sacerdoti, F.D., Salmon, J.K., 2006. Scalable algorithms for molecular dynamics simulations on commodity clusters. In Proceedings of the 2006 ACM/IEEE Conference on Supercomputing. 84, 43.

Chaudhuri, S., Banerjee, A., Basu, K., Sengupta, B., Sengupta, P.K., 2007. Interaction of flavonoids with red blood cell membrane lipids and proteins: antioxidant and antihemolytic effects. International Journal of Biological Macromolecules. 41, 42-48.

Chaveerach, U., Meenongwa, A., Trongpanich, Y., Soikum, C., Chaveerach, P., 2010. DNA binding and cleavage behaviors of copper (II) complexes with amidino-O-methylurea and N-methylphenyl-amidino-O-methylurea, and their antibacterial activities. Polyhedron. 29, 731-738.

Chi, Z., Liu, R., Sun, Y., Wang, M., Zhang, P., Gao, C., 2010. Investigation on the toxic interaction of toluidine blue with calf thymus DNA. Journal of Hazardous materials. 175, 274-278.

Darzynkiewicz, K., Kapuscinski, J., 1990. Flow Cytometry and Sorting, second ed.,Wiley-Liss, New York. 291-314.

Das, P., Chakrabarty, A., Haldar, B., Mallick, A., Chattopadhyay, N., 2007. Effect of

cyclodextrinnanocavity confinement on the photophysics of a β-carboline analogue: a spectroscopic study. The Journal of Physical Chemistry B. 111, 7401-7408.

Fei, Y., Lu, G., Fan, G., Wu, Y., 2009. Spectroscopic studies on the binding of a new quinolone antibacterial agent: sinafloxacin to DNA. Analytical Sciences. 25, 1333-1338.

Ganguly, A., Ghosh, S., Guchhait, N., 2015. Spectroscopic and viscometric elucidation of the interaction between a potential chloride channel blocker and calf-thymus DNA: the effect of medium ionic strength on the binding mode. Physical Chemistry Chemical Physics. 17, 483-492.

Ghosh, S., Kundu, P., Paul, B.K., Chattopadhyay, N., 2014. Binding of an anionic fluorescent probe with calf thymus DNA and effect of salt on the probe-DNA binding: a spectroscopic and molecular docking investigation. RSC Advances. 4, 63549-63558.

Georgiou, C.D., Papapostolou, I., Grintzalis, K., 2009. Protocol for the quantitative assessment of DNA concentration and damage (fragmentation and nicks). Nature Protocols. 4, 125-131.

Ghosh, N., Mondal, R., Mukherjee, S., 2015. Inverse temperature dependence in static quenching versus calorimetric exploration: binding interaction of chloramphenicol to β-lactoglobulin. Langmuir. 31, 8074-8080.

Ghosh, S., Mallick, S., Das, U., Verma, A., Pal, U., Chatterjee, S., Nandy, A., Saha, K.D., Maiti, N.C., Baishya, B., Kumar, G.S., 2018. Curcumin stably interacts with DNA hairpin through minor groove binding and demonstrates enhanced cytotoxicity in combination with FdU nucleotides. Biochimica et Biophysica Acta (BBA)-General Subjects. 1862, 485-494.

Guharay, J., Chaudhuri, R., Chakrabarti, A., Sengupta, P.K., 1997. Excited state proton transfer fluorescence of 3-hydroxyflavone in model membranes. Spectrochimica Acta Part A: Molecular and Biomolecular Spectroscopy. 53, 457-462.

Hameed, H., Aydin, S., Başaran, N., 2016. Sinapic acid: is it safe for humans?. Fabad Journal of Pharmaceutical Sciences, 41, 39.

Han, X.L., Mei, P., Liu, Y., Xiao, Q., Jiang, F.L., Li, R., 2009. Binding interaction of quinclorac with bovine serum albumin: a biophysical study. Spectrochimica Acta Part A: Molecular and Biomolecular Spectroscopy. 74, 781-787.

Husain, M.A., Ishqi, H.M., Rehman, S.U., Sarwar, T., Afrin, S., Rahman, Y., Tabish, M., 2017. Elucidating the interaction of sulindac with calf thymus DNA: biophysical and in silico molecular modelling approach. New Journal of Chemistry. 41, 14924-14935.

Husain, M.A., Yaseen, Z., Rehman, S.U., Sarwar, T., Tabish, M., 2013. Naproxen intercalates with DNA and causes photocleavage through ROS generation. The FEBS journal. 280, 6569-6580.

Jana, B., Senapati, S., Ghosh, D., Bose, D., Chattopadhyay, N., 2012. Spectroscopic exploration of mode of binding of ctDNA with 3-hydroxyflavone: a contrast to the mode of binding with flavonoids having additional hydroxyl groups. The Journal of Physical Chemistry B. 116, 639-645.

Kumar, C.V., Turner, R.S., Asuncion, E.H., 1993. Groove binding of a styrylcyanine dye to the DNA double helix: the salt effect. Journal of Photochemistry and Photobiology A: Chemistry. 74, 231-238.

Kumar, N., Goel, N., 2019. Phenolic acids: Natural versatile molecules with promising therapeutic applications. Biotechnology Reports. 24, e00370.

Lakowicz, J. R., 2006. Principles of Fluorescence Spectroscopy, 3rd ed.; Plenum: New York. 270-350.

Lehrer, S., 1971. Solute perturbation of protein fluorescence. Quenching of the tryptophyl fluorescence of model compounds and of lysozyme by iodide ion. Biochemistry. 10, 3254-3263.

Lepecq, J.B., Paoletti, C., 1967. A fluorescent complex between ethidium bromide and nucleic acids: physical-chemical characterization. Journal of Molecular Biology. 27, 87-106.

Li, X.L., Hu, Y.J., Wang, H., Yu, B.Q., Yue, H.L., 2012. Molecular spectroscopy evidence of berberine binding to DNA: comparative binding and thermodynamic profile of intercalation. Biomacromolecules. 13, 873-880.

Ling, X., Zhong, W., Huang, Q., Ni, K., 2008. Spectroscopic studies on the interaction of pazufloxacin with calf thymus DNA. Journal of Photochemistry and Photobiology B: Biology. 93, 172-176.

Lu, C., Yao, S., Lin, N., 2001. Studies on reactions of oxidizing sulfur-sulfur three electron bond complexes and reducing α-amino radicals derived from OH reaction with methionine in aqueous solution. Biochimica et Biophysica Acta (BBA)-General Subjects. 1525, 89-96.

Ma, X., Chen, M., Wu, Y., Li, X., Zhang, S., 2016. Studies on the electrochemical behavior of chlorogenic acid and its interaction with DNA at a graphene modified electrode. Int. J. Electrochem. Sci. 11, 8499-8511.

Ma, Y., Zhang, G., Pan, J., 2012. Spectroscopic studies of DNA interactions with food colorant indigo carmine with the use of ethidium bromide as a fluorescence probe. Journal of Agricultural and Food Chemistry. 60, 10867-10875.

Manojkumar, K., PrabhuCharan, K.T., Sivaramakrishna, A., Jha, P.C., Khedkar, V.M., Siva, R., Jayaraman, G., Vijayakrishna, K., 2015. Biophysical characterization and molecular docking studies of imidazolium based polyelectrolytes-DNA complexes: Role of hydrophobicity. Biomacromolecules. 16, 894-903.

Mati, S.S., Roy, S.S., Chall, S., Bhattacharya, S., Bhattacharya, S.C., 2013. Unveiling the groove binding mechanism of a biocompatible naphthalimide-based organoselenocyanate with calf thymus DNA: an "ex vivo" fluorescence imaging application appended by biophysical experiments and molecular docking simulations. The Journal of Physical Chemistry B. 117, 14655-14665.

Modukuru, N.K., Snow, K.J., Perrin, B.S., Thota, J., Kumar, C.V., 2005. Contributions of a long side chain to the binding affinity of an anthracene derivative to DNA. The Journal of Physical Chemistry B. 109, 11810-11818.

Morris, G.M., Huey, R., Lindstrom, W., Sanner, M.F., Belew, R.K., Goodsell, D.S., Olson, A.J., 2009. AutoDock4 and AutoDockTools4: Automated docking with selective receptor flexibility. Journal of Computational Chemistry. 30, 2785-2791.

Nayab, P.S., Pulaganti, M., Chitta, S.K., Rahisuddin, 2016. Multi-spectroscopic and molecular docking studies on the interaction of new phthalimides with calf-thymus DNA: In vitro free radical scavenging activities. Spectroscopy Letters. 49, 108-117.

Olmsted III, J., Kearns, D.R., 1977. Mechanism of ethidium bromide fluorescence enhancement on binding to nucleic acids. Biochemistry. 16, 3647-3654.

Pal, U., Pramanik, S.K., Bhattacharya, B., Banerji, B., C Maiti, N., 2016. Binding interaction of a gamma-aminobutyric acid derivative with serum albumin: an insight by fluorescence and molecular modeling analysis. Springer Plus. 5, 1-17.

Paul, B.K., Guchhait, N., 2011. Exploring the strength, mode, dynamics, and kinetics of binding interaction of a cationic biological photosensitizer with DNA: implication on dissociation of the drug-DNA complex via detergent sequestration. The Journal of Physical Chemistry B. 115, 11938-11949.

Qais, F.A., Abdullah, K.M., Alam, M.M., Naseem, I., Ahmad, I., 2017. Interaction of capsaicin with calf thymus DNA: A multi-spectroscopic and molecular modelling study. International Journal of Biological Macromolecules. 97, 392-402.

Ranjbar, B., Gill, P., 2009. Circular dichroism techniques: biomolecular and nanostructural analyses a review. Chemical Biology and Drug Design. 74, 101-120.

Rehman, S.U., Yaseen, Z., Husain, M.A., Sarwar, T., Ishqi, H.M. and Tabish, M., 2014.Interaction of 6 mercaptopurine with calf thymus DNA-deciphering the binding mode and photoinduced DNA damage. Plos One. 9, e93913.

Ross, P.D., Subramanian, S., 1981. Thermodynamics of protein association reactions: forces contributing to stability. Biochemistry. 20, 3096-3102.

Sarkar, D., Das, P., Basak, S., Chattopadhyay, N., 2008. Binding interaction of cationic phenazinium dyes with calf thymus DNA: a comparative study. The Journal of Physical Chemistry B. 112, 9243-9249.

Sarwar, T., Ishqi, H.M., Rehman, S.U., Husain, M.A., Rahman, Y., Tabish, M., 2017.Caffeic acid binds to the minor groove of calf thymus DNA: A multi-spectroscopic, thermodynamics and molecular modelling study. International Journal of Biological Macromolecules. 98, 319-328.

Sengupta, P., Ganguly, A., Bose, A., 2018. A phenolic acid based colourimetric 'naked-eye'chemosensor for the rapid detection of Cu (II) ions. Spectrochimica Acta Part A: Molecular and Biomolecular Spectroscopy, 198, 204-211.

Sengupta, P., Pal, U., Mondal, P., Bose, A., 2019. Multi-spectroscopic and computational evaluation on the binding of sinapic acid and its Cu (II) complex with bovine serum albumin. Food chemistry. 301, 125254.

Sengupta, P., Sardar, P.S., Roy, P., Dasgupta, S., Bose, A., 2018. Investigation on the interaction of Rutin with serum albumins: Insights from spectroscopic and molecular docking techniques. Journal of Photochemistry and Photobiology B: Biology. 183, 101-110.

Shyamala, T., Mishra, A.K., 2004.Ground-and Excited-state Proton Transfer Reaction of 3-Hydroxyflavone in Dimyristoylphosphatidylcholine Liposome Membrane. Photochemistry and Photobiology, 80, 309-315.

Smyk, B., Drabent, R., 1989. Spectroscopic investigation of the equilibria of the ionic forms of sinapic acid. Analyst. 114, 723-726.

Thomas, R.K., Sukumaran, S., Sudarsanakumar, C., 2019. An insight into the comparative binding affinities of chlorogenic acid functionalized gold and silver nanoparticles with ctDNA along with its cytotoxicity analysis. Journal of Molecular Liquids. 287, 110911.

Tian, F.F., Jiang, F.L., Han, X.L., Xiang, C., Ge, Y.S., Li, J.H., Zhang, Y., Li, R., Ding, X.L.,

Liu, Y., 2010. Synthesis of a novel hydrazone derivative and biophysical studies of its interactions with bovine serum albumin by spectroscopic, electrochemical, and molecular docking methods. The Journal of Physical Chemistry B, 114, 14842-14853.

Trott, O., Olson, A.J., 2010. AutoDockVina: improving the speed and accuracy of docking with a new scoring function, efficient optimization, and multithreading. Journal of Computational Chemistry. 31, 455-461.

Wang, X., Cui, F., 2018. Binding characteristics of imidazolium-based ionic liquids with calf thymus DNA: Spectroscopy studies. Journal of Fluorine Chemistry. 213, 68-73.

Yoon, B.H., Jung, J.W., Lee, J.J., Cho, Y.W., Jang, C.G., Jin, C., Oh, T.H. and Ryu, J.H., 2007. Anxiolytic-like effects of sinapic acid in mice. Life Sciences. 81, 234-240.

Yun, K.J., Koh, D.J., Kim, S.H., Park, S.J., Ryu, J.H., Kim, D.G., Lee, J.Y., Lee, K.T., 2008. Anti-inflammatory effects of sinapic acid through the suppression of inducible nitric oxide synthase, cyclooxygase-2, and proinflammatory cytokines expressions via nuclear factor-κB inactivation. Journal of Agricultural and Food Chemistry. 56, 10265-10272.

Zhang, G., Wang, L., Zhou, X., Li, Y., Gong, D., 2014. Binding characteristics of sodium saccharin with calf thymus DNA in vitro. Journal of Agricultural and Food Chemistry. 62, 991-1000.

Zhang, S., Sun, X., Qu, F., Kong, R., 2013. Molecular spectroscopic studies on the interaction of ferulic acid with calf thymus DNA. Spectrochimica Acta Part A: Molecular and Biomolecular Spectroscopy. 112, 78-83.

Zhou, X., Zhang, G., Pan, J., 2015. Groove binding interaction between daphnetin and calf thymus DNA. International Journal of Biological Macromolecules. 74, 185-194.

Zou, Y., Kim, A.R., Kim, J.E., Choi, J.S., Chung, H.Y., 2002. Peroxynitrite scavenging activity of sinapic acid (3, 5-dimethoxy-4-hydroxycinnamic acid) isolated from Brassica juncea. Journal of Agricultural and Food Chemistry. 50, 5884-5890.